Selective Demethoxylation of Guaiacols to Phenols using Supported MoO 3 Catalysts

Yang, Huaizhou; Yin, Wang; Zhu, Xiaotian; Deuss, Peter J.; Heeres, Hero J.

IMPORTANT NOTE: You are advised to consult the publisher's version (publisher's PDF) if you wish to cite from it. Please check the document version below.

Document Version
Publisher's PDF, also known as Version of record

Link to publication in University of Groningen/UMCG research database

Selective Demethoxylation of Guaiacols to Phenols using Supported MoO3 Catalysts

Huaizhou Yang+,[a] Wang Yin+,[a, b] Xiaotian Zhu,[c] Peter J. Deuss,[a] and Hero J. Heeres*[a]

Lignin-derived monomers with methoxy substituents are abundantly present in bioliquids derived from lignocellulosic biomass. Examples are the products obtained from the reductive catalytic fractionation of lignin (RCF) and pyrolysis of lignocellulosic biomass and hydrotreated products thereof. An attractive valorization step for these liquids involves demethoxylation to obtain alkylated phenols through selective catalytic hydrodeoxygenation (HDO). Within the context of sustainable chemistry, there is a strong drive to use cheap, non-precious metal catalysts for this purpose. In this study, the HDO of guaiacol (5 wt% in toluene) was investigated in a continuous fixed-bed reactor at 380 °C, 20 bar over supported MoO3 catalysts. MoO3 (5 %) supported on TiO2 (P25) was shown to give superior performance compared with MoO3 supported on anatase TiO2, Al2O3, SiO2, Nb2O5, CeO2, and ZrO2. Additional studies involving variation of the Mo loading and process conditions were performed, and the highest selectivity to demethoxylated phenolics like phenol and methylated phenols was 82 % at 97 % conversion of guaiacol. Both 4-n-propylguaiacol and a realistic guaiacols-rich feed isolated from a representative pyrolysis oil were also successfully demethoxylated with the 5 % MoO3/TiO2 catalyst.

1. Introduction

The use of renewable carbon such as biomass for the production of biobased chemicals is essential to green up the chemical industry. Nowadays, phenol and alkylphenols are in great demand and produced from fossil resources.[1,2] The production of biobased phenolics from lignocellulosic biomass has been investigated, and many promising (catalytic) options have been identified. For instance, fast pyrolysis technology may be used to obtain a pyrolysis liquid enriched in phenolic compounds.[3,4] Such liquids can be further concentrated by fractionation using liquid-liquid extraction and distillation.[4–7] This fractionation process has been demonstrated on a pilot plant scale.[8] The phenolic fractions typically consist of mixtures of phenolic compounds with different amounts of methoxy substituents (guaiacols and syringols), which hinders their valorization.[5,9] Selective catalytic demethoxylation is an effective way to convert this mixture of lignin-derived methoxylated monomers to alkyl substituted phenolics.[10,11] Typically, a catalytic hydrodeoxygenation (HDO) approach using a supported catalyst in combination with hydrogen gas is applied. Guaiacol is a well-known model compound for catalytic demethoxylation studies, particularly when considering that it is present in significant amounts in many bioliquids derived from lignocellulosic biomass and lignin conversions.[12,13]

Selective demethoxylation of guaiacol using an HDO approach is challenging because the C−O bond-dissociation energies of the phenolic OH group and the methoxy group (Ph-OMe) are very similar and much higher than the PhO−Me bond.[14,15] Several exploratory catalyst studies for the selective conversion of guaiacol to demethoxylated phenolics have been reported in the literature. Examples are precious metal catalysts like Pt−Sn/CNF/Inconel,[16] Pd/C,[17] TiO2 supported Au, Ag, and Ru catalysts[18–22] but also cheaper Fe-based catalysts such as FeOx/CeO2,[23] supported Ni catalysts,[24,25] and Mo oxide catalysts[14,26–30], as shown in Table 1. Both batch set-up and fixed-bed reactors were used in previous studies. Typical temperatures are between 240 and 400 °C, with hydrogen pressures between 0.1 and 4 MPa. The use of precious metal catalysts, such as Pt−Sn/CNF/Inconel, Pd/C, and Au/TiO2, have resulted in high guaiacol conversion as well as good selectivities, and the yield of demethoxylated phenolics was as high as 84 % for Au/TiO2 using 4-n-propylguaiacol as the reactant.[20] Support effect studies for the latter catalyst show that Au supported on TiO2 (P25, containing anatase and rutile) performs better than with supports like anatase TiO2, rutile TiO2, MgO,

[a] H. Yang,+ Dr. W. Yin,+ Prof. P. J. Deuss, Prof. H. J. Heeres
Department of Chemical Engineering
ENTEG
University of Groningen
9747 AG, Groningen (The Netherlands)
E-mail: h.j.heeres@rug.nl

[b] Dr. W. Yin+
Fujian Universities Engineering Research Center of Reactive Distillation Technology
College of Chemical Engineering
Fuzhou University
Fuzhou 350116, Fujian (P. R. China)

[c] Dr. X. Zhu
Zernike Institute for Advanced Materials
University of Groningen
9747 AG Groningen (The Netherlands)

[+] These authors contributed equally to this paper

ChemCatChem

Research Article
doi.org/10.1002/cctc.202200297

**Chemistry
Europe**
European Chemical
Societies Publishing

Table 1. Overview of selected catalyst families for the conversion of guaiacols to demethoxylated phenolics using heterogeneous catalysts.

Feed	Reaction conditions	Catalyst	Conversion [%]	Selectivity to demethoxylated phenolics [%]	Ref
Guaiacol	Fixed-bed, 400 °C, 0.1 MPa, WHSV = 0.31 h^{-1}	Pt–Sn/CNF/ Inconel	97[a]	84[a]	[16]
Guaiacol	Fixed-bed, 350 °C, 0.4 kPa partial pressure of guaiacol, 40 kPa H_2, W/F = 0.15 s·g·STP mL^{-1}	Pd/C	99[b]	80[b]	[17]
Guaiacol	Batch, 300 °C, 3 MPa H_2, 700 rpm, 3 h	Au/TiO_2	43[a]	87[a]	[18]
Guaiacol	Fixed-bed, 300 °C, 2.7 kPa partial pressure of guaiacol, 4 MPa H_2	Au/TiO_2	92[a]	79[a]	[19]
4-propylguaiacol	Batch, 350 °C, 5 MPa H_2, 2 h	Au/TiO_2	100[a]	84[a]	[20]
Guaiacol	Batch, 300 °C, 3 MPa H_2, 700 rpm, 1 h	Ag/TiO_2	41[a]	77[a]	[21]
Guaiacol	Batch, 240 °C, 1 MPa H_2, 700 rpm, 1 h	Ru/Cl/TiO_2	45[a]	65[a]	[22]
Guaiacol	Batch, 300 °C, 4 MPa H_2, 500 rpm, 2 h	Ni/TiO_2	48[a]	94[a]	[24]
Guaiacol	Fixed-bed, 350 °C, 0.5 MPa, WHSV = 10 h^{-1}	Ni/TiO_2	50[a]	76[a]	[25]
4-propylguaiacol	Fixed-bed, 285 °C, 0.1 MPa, WHSV = 6 h^{-1}	Ni/SiO_2	94[a]	89[a]	[31]
Pine wood derived lignin monomers	Fixed-bed, 285 °C, 0.1 MPa, WHSV = 6 h^{-1}	Ni/SiO_2	92[a]	88[a]	[31]
Guaiacol	Fixed-bed, 400 °C, 0.1 MPa, W/F = 1.21 g·h·mol_{total}^{-1}	FeO_x/CeO_2	100[b]	87[b]	[23]
Guaiacol	Fixed-bed, 375 °C, 0.1 MPa, WHSV = 0.71 h^{-1}	CeO_2-ZrO_2	59[a]	92[a]	[32]
Guaiacol	Fixed-bed, 350 °C, 1.5 kPa partial pressure of guaiacol, 99.8 kPa H_2, WHSV = 3.55 h^{-1}	MoO_3	98[b]	30[b]	[14]
Guaiacol	Batch, 340 °C, 0.5 MPa H_2 + 3 MPa N_2, 800 rpm, 6 h	MoO_3	98[c]	13[c]	[26]
Guaiacol	Batch, 300 °C, 4 MPa H_2, 1000 rpm, 4 h	MoO_3	96[a]	97[a]	[27]
Guaiacol	Batch, 300 °C, 3 MPa H_2, 600 rpm, 3 h	MoO_2/AC	98[d]	91[d]	[28]
Guaiacol	Fixed-bed, 400 °C, 4 MPa, WHSV = 14.9 h^{-1}	MoO_3/AC	99[c]	71[c]	[29]
4-propylguaiacol	Fixed-bed, 350 °C, 100 kPa H_2, WHSV = 2 h^{-1}	MoO_3/SiO_2	82[d]	76[d]	[30]
4-propylguaiacol	Fixed-bed, 350 °C, 9 MPa, WHSV = 80 h^{-1}	MoP/SiO_2	96[a]	99[a]	[33]
Guaiacol	Batch, 300 °C, 5 MPa H_2, 4 h	MoN	92[a]	92[a]	[34]
Guaiacol	Batch, 320 °C, 3.4 MPa H_2, 1000 rpm, 4 h	Mo_2C/AC	100[a]	88[a]	[35]
Guaiacol	Batch, 300 °C, 0.5 MPa H_2, 2 h	MoC_x/C	99[a]	84[a]	[1]

Conversion and selectivity were calculated based on [a] molar basis, [b] carbon basis, and [c] weight basis; [d] not reported in original publication.

SiO_2, $MgCr_2O_4$, and $MgCuCr_2O_4$. As a result, precious metals supported on TiO_2 have received considerable attention including those based on Au, Ag, and Ru. Due to a strong drive to use alternatives to these precious metals, the use of Ni-based catalysts (TiO_2 as support, 3–5% Ni loading) has also been investigated (Table 1). The use of Ni catalyst (Ni/SiO_2) with high Ni loading (64%) resulted in excellent performance for both model compound and real feed derived from pine wood (enriched in 4-n-propylguaiacol). In addition, good results were obtained using FeO_x/CeO_2 and the support alone (CeO_2–ZrO_2) with conversion and selectivity levels similar or even slightly exceeding those of precious metal catalysts. Mo based catalysts, in the form of oxides, phosphides, nitrides, and carbides, have been used for the catalytic demethoxylation, though mainly in batch set-ups (Table 1). High yields (83-95%) of demethoxylated phenols were obtained for molybdenum phosphide, nitride, and carbide catalysts. MoO_3, either as such or supported on activated carbon (AC) or SiO_2, has also been tested in exploratory catalyst screening studies. Good yields have been reported when performing the experiments in batch set-ups (12–93%), though a considerable reduction was reported when using continuous flow reactors (29–70%). However, support screening studies have not been performed for MoO_3 supported catalysts for guaiacol demethoxylation, and particularly the use of TiO_2 has not been explored. This is of high interest as this support has shown to be the best one for precious metal catalysts (*vide supra*). Finally, demethoxylation studies with Mo-based catalysts have been reported using model components

only, and the performance of these catalysts for demethoxylation of real bioliquids enriched in guaiacols is unknown and an absolute novelty of this paper.

To overcome the gap in the current literature, a series of MoO_3 catalysts on different oxidic supports like TiO_2 (P25, anatase), Al_2O_3, SiO_2, Nb_2O_5, CeO_2, and ZrO_2 was prepared, characterized, and evaluated in a continuous fixed-bed reactor for the demethoxylation of guaiacol. The influence of the support, MoO_3 loading as well as process conditions on catalyst performance were studied. Model compounds and feeds were incrementally advanced from guaiacol to 4-n-propylguaiacol to a mixture of methoxylated phenolics isolated from pyrolysis oil by fractionation.

2. Results and discussion

2.1. Exploratory catalytic screening experiments

In the first stage of experimentation, the catalytic conversion of guaiacol was performed using a series of supported MoO_3 catalysts (P25 and anatase TiO_2, Al_2O_3, SiO_2, Nb_2O_5, CeO_2, and ZrO_2). All catalysts were prepared using an incipient wetness procedure aiming at a MoO_3 loading of 5 wt%. Relevant catalyst characterization data (ICP-OES, N_2 physisorption, and oxygen storage capacity) are provided in Table 2.

Catalytic experiments were carried out in a continuous down-flow packed-bed reactor at 380 °C, 20 bar of H_2 flow

ChemCatChem

Research Article
doi.org/10.1002/cctc.202200297

Chemistry
Europe
European Chemical
Societies Publishing

Table 2. Relevant properties of the MoO$_3$ catalysts on different supports.

Catalysts	MoO$_3$ content[a] [wt.%]	S$_{BET}$[b] [m^2/g]	Pore volume[b] [cm^3/g]	d$_{pores}$[b] [nm]	Oxygen vacancies[c] [μmol/g]
5% MoO$_3$/TiO$_2$ P25	4.5	61	0.237	16.0	255
5% MoO$_3$/A-TiO$_2$	4.8	13	0.097	29.1	49
5% MoO$_3$/ZrO$_2$	4.5	7	0.037	18.8	45
5% MoO$_3$/Nb$_2$O$_5$	4.4	7	0.046	22.4	9
5% MoO$_3$/CeO$_2$	5.0	27	0.133	17.4	113
5% MoO$_3$/Al$_2$O$_3$	5.3	85	0.441	22.0	60
5% MoO$_3$/SiO$_2$	5.0	137	0.871	25.1	9

[a] Determined by ICP-OES; [b] Determined by N$_2$ physisorption; [c] Determined by oxygen storage capacity measurement.
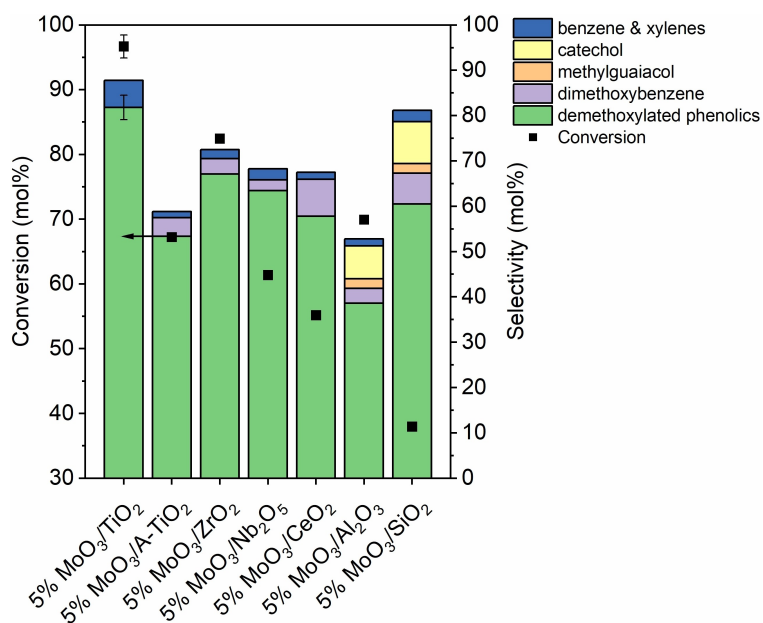
Figure 1. Conversion and selectivity for the demethoxylation of guaiacol using supported MoO$_3$ (5%) catalysts (T = 380 °C, P = 20 bar, WHSV = 0.5 h^{-1}, 5 wt% guaiacol in toluene, and TOS = 4 h). Detailed product distributions are shown in Figure S2.

(10 mL/min), with 5 wt% guaiacol dissolved in toluene as a reactant and a WHSV of 0.5 h^{-1}. An example of a representative conversion versus time on stream (TOS) profile is given in Figure S1. After about 4 h, a steady-state operation was achieved and the guaiacol conversion became independent of the TOS. For all exploratory catalyst screening experiments, the conversion and selectivity after 4 h TOS is provided.

The conversion and selectivity data for all catalysts are provided in Figure 1, and a strong effect of the support on catalytic performance was observed. The highest conversion was obtained using the 5% MoO$_3$ on TiO$_2$ (P25, 97%), whereas the worst performance was obtained when using the SiO$_2$ support (38%). Of interest is the observation that anatase TiO$_2$ as the support performs worse than TiO$_2$ (P25).

The main products of the reactions are the desired demethoxylated phenols, including phenol and alkylated phenols like methyl-, dimethyl-, and trimethylphenol, whereas also minor amounts of catechol and aromatics like xylenes and benzene were detected. A schematic overview of the main reactions is given in Scheme 1. The product portfolio shows that demethoxylation, as well as methyl transfer, occurs to a significant
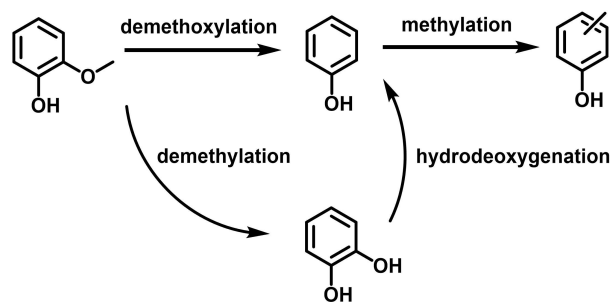
Scheme 1. Simplified reaction network for the catalytic hydrotreatment of guaiacol.

extent. Overhydrogenation of the C–C double bonds in aromatic rings to saturated alcohols and (cyclic) alkanes was not observed. Anisole, formed by cleavage of the Ph–OH bond, was also not detected. A blank reaction with toluene only was performed to determine whether aromatics like xylenes and benzene were formed from the solvent (toluene). Hardly any

ChemCatChem

Research Article
doi.org/10.1002/cctc.202200297

Chemistry
Europe

European Chemical
Societies Publishing

Table 3. Relevant properties of the supported MoO_3 catalysts.

Catalysts	MoO_3 content[a] [wt%]	Physisorption data[b] S_{BET} [m²/g]	Pore volume [cm³/g]	d_{pores} [nm]	Chemisorption data[c] Total [μmol NH₃/g]	Weak[d]	Medium[e]	Strong[f]	Oxygen vacancies[g] [μmol/g]
TiO_2	–	55	0.205	16.7	267	142	125	0	4
1% MoO_3/TiO_2	1.0	57	0.292	21.1	241	139	102	0	40
3% MoO_3/TiO_2	3.0	57	0.278	20.9	235	69	165	1	143
5% MoO_3/TiO_2	4.5	61	0.237	16.0	257	80	174	3	255
10% MoO_3/TiO_2	10.2	55	0.202	14.2	260	81	149	30	446
15% MoO_3/TiO_2	15.4	52	0.217	17.1	264	77	132	55	465
20% MoO_3/TiO_2	20.4	51	0.197	15.5	251	103	99	50	437
MoO_3	–	2	0.002	63.6	43	8	0	35	2

[a] Determined by ICP-OES, [b] Determined by N_2 physisorption; [c] Determined by NH_3-TPD; [d] weak acidic sites (temperature range 100–250 °C); [e] medium acidic sites (temperature range 250–350 °C); [f] strong acidic sites (temperature range 350–380 °C); [g] Determined by oxygen storage capacity measurement, see experimental section for details.

benzene and xylenes were detected, indicating that this pathway is not occurring to a significant extent.

The highest selectivity for (alkylated) phenols of 82% in the screening experiments was obtained using 5% MoO_3 on TiO_2 (P25), giving a yield of desired demethoxylated compounds of 79%. This yield is considerably higher than found for literature data for experiments performed in continuous set-ups using guaiacol as the feed and Mo-based catalysts (29% for unsupported MoO_3 and 70% for MoO_3/AC, Table 1) and illustrates the good performance of TiO_2 as support for demethoxylation catalysts.

2.2. Systematic studies using MoO_3 supported on TiO_2

A series of MoO_3 catalysts supported on TiO_2 (P25), the best support in the catalyst screening study, with different MoO_3 loadings (1-20 wt%) was prepared using incipient wetness impregnation. The catalysts were characterized in detail (ICP-OES, N_2 physisorption, oxygen storage capacity, XRD, H_2-TPR, NH_3-TPD, and HADDF-STEM) and tested for the demethoxylation of guaiacol and a bioliquid enriched in guaiacol (Pyoil) in toluene as well as for 4-*n*-propylguaiacol in the absence of a solvent.
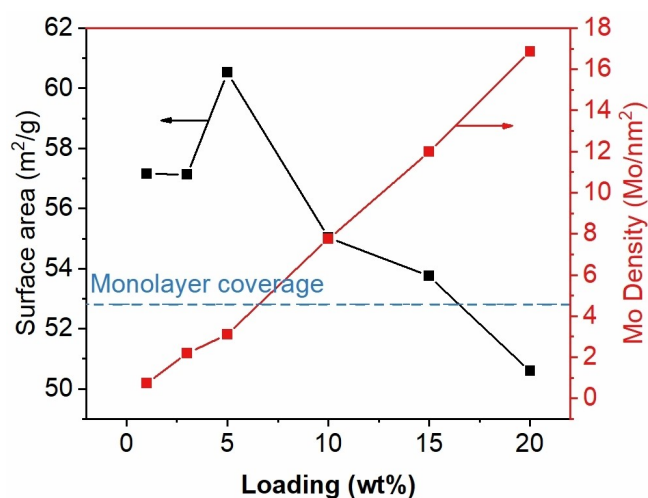
2.2.1. Catalyst characterization

The Mo content of the MoO_3/TiO_2 catalysts was determined by ICP-OES (Table 3) and revealed that the MoO_3 contents are close to the theoretical values. XRD was used to examine the phases and crystallinity (Figure S3). As expected, the XRD pattern of the bulk TiO_2 (P25) shows the presence of both anatase and rutile phases. At low MoO_3 loadings (1-5%), additional peaks from Mo phases are absent. These findings indicate that highly dispersed Mo species are present at low MoO_3 loading, consistent with literature data.[37,38] However, at higher loadings, and particularly at loadings above 10%, peaks from MoO_3 crystallites ($2\theta =$ 12.8°, 23.4°, and 27.4°, peak at 27.4° overlapping with rutile TiO_2) are observed. The MoO_3 size for the samples with clear

XRD peaks for this phase was calculated using the Scherrer equation and found to be between 32–42 nm.

The specific surface area as determined by N_2 physisorption experiments versus the MoO_3-loading shows a volcano type plot with a maximum surface area of 61 m²/g for a MoO_3 loading of 5 wt% (Figure 2). The increase in surface area when going from a 1 to 5% MoO_3 loading is likely related to the presence of highly dispersed Mo species on the TiO_2 nanoparticles in the calcination step. It is well known that the TiO_2 structure tends to collapse during calcination, resulting in a reduction of the surface area. In the presence of highly dispersed metal nanoparticles, the structure is stabilized, leading to less structural damage and collapse during calcination.[37] At higher loadings and particularly above monolayer coverage, the surface area decreases because of the formation of crystalline Mo phases that gradually fill the pores.[37,39]

The molybdenum density (Mo/nm²) was calculated using the Mo content and the surface area.[40] The Mo density is below monolayer coverage (about 5 Mo/nm²) when the loading is below 5%.[37,41,42] The molybdenum species are expected to be

Figure 2. BET surface areas and Mo densities versus MoO_3 loading for the 1–20% MoO_3/TiO_2 catalysts.
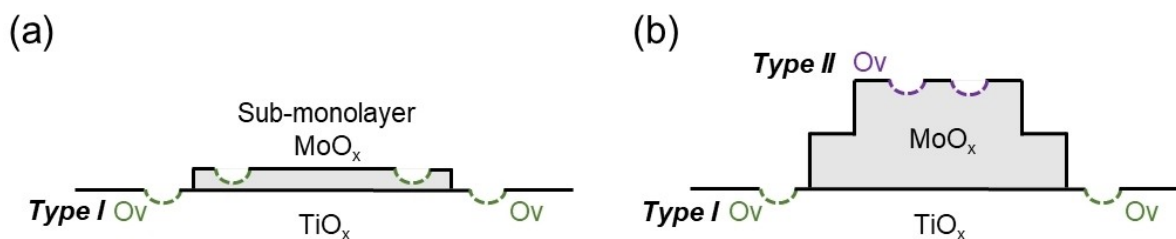
ChemCatChem

Research Article
doi.org/10.1002/cctc.202200297

**Chemistry
Europe**
European Chemical
Societies Publishing

Figure 3. Different oxygen vacancy sites of (a) 1–5% MoO_3/TiO_2, (b) 10–20% MoO_3/TiO_2.

presented as isolated or small aggregates at such low Mo loading, as reported in the literature for MoO_3/TiO_2 (anatase).[38]

The reducibility of the materials was investigated by H_2-TPR (Figure S4). TiO_2 (P25) does not show significant reduction peaks in the range of 50–900°C, in line with literature data for H_2-TPR measurements on TiO_2 supports.[43,44] For MoO_3/TiO_2 materials with a low Mo loading (1-5% MoO_3), two peaks are visible (α and γ). The first broad one (ca. 400°C) is associated with the reduction of Mo^{6+} to Mo^{4+} (α), and the second one (ca. 750°C) with a further reduction of Mo^{4+} to Mo^0 (γ).[41,45,46] The peak for the first reduction step extends considerably to higher temperatures, indicating $Mo^{6+} \rightarrow Mo^{5+} \rightarrow Mo^{4+}$ and $Ti^{4+} \rightarrow Ti^{3+}$ transformations. When the Mo loading above monolayer coverage (10 wt% MoO_3), the Mo^{6+} species are present in both a tetrahedral and octahedral coordination mode.[45] As a result, two additional peaks (β and δ) showed up during reduction, which could be assigned to the reduction of octahedral coordinated Mo^{6+} to Mo^{4+} (β feature) and further reduction to Mo^0 (δ feature), respectively. Of interest is the observation that Mo is more difficult to reduce at higher Mo loadings, consistent with the reduction behavior of MoO_3/TiO_2 (anatase) catalysts described in the literature.[38]

Oxygen vacancies (Ov) have been proposed to play a role in the molecular mechanism for the demethoxylation of guaiacol when using MoO_x supported catalysts (Figure 3).[14,21,47]

As such, the quantification of the amounts of oxygen vacancies in the materials was performed by oxygen pulse chemisorption. The concentration of Ov versus the MoO_3 loading is given in Figure 4 and shows a volcano-type profile with a maximum at MoO_3 loadings between 10 and 20 wt%. The Ov concentrations for the individual components (bulk TiO_2 and MoO_3) are by far lower. Liu et al. performed studies on Ag/TiO_2 as a demethoxylation catalyst and proposed that Ov are formed by the reduction of the TiO_2 surface by spillover hydrogen.[21] Like Ag, reduced MoO_x species can activate hydrogen and produce spillover hydrogen to reduce the surface of the TiO_2 support.[48,49] However, oxygen vacancies may also be present on the MoO_x crystallites by partial reduction of MoO_3.[14] This is also confirmed by the TPR data for the catalyst samples, particularly at high Mo loading, see Figure S4 for details. A schematic representation of possible Ov sites is given in Figure 3. The profile of the Ov concentration versus the Mo loading as given in Figure 4 can be explained by considering the type of MoO_3 species present at the surface. At low Mo loadings, these are considered to be present as small isolated
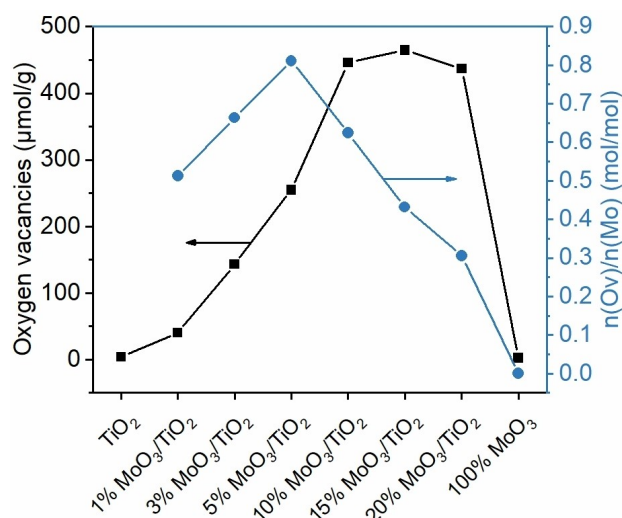

Figure 4. Oxygen vacancy concentrations and the ratio between the concentration of Ov (n(Ov), μmol/g) and the Mo content in the catalyst (n(Mo), μmol/g), measured by oxygen pulse chemisorption at 380°C and ICP-OES, respectively. Catalysts were reduced *in-situ* at 380°C under 5% H_2/Ar for 1 h.

MoO_3 or slightly agglomerated MoO_3 clusters. The amount of Ov increases with the Mo loading as more Mo species are reduced, and thus higher amounts of spillover H is formed which are required for Ov formation. At Mo loadings above about 10%, surface coverage is above monolayer concentrations, and larger MoO_x crystallites are formed. These are more difficult to be reduced at 380°C, leading to a reduction in the Ov concentrations.

NH_3-TPD was performed to quantify the surface acidity of the catalysts used in this study, which is known to affect catalyst performance for demethylation reactions[20,50] The NH_3-TPD profiles and quantification results are shown in Figure S5 and Table 3. Acidity appears to be rather independent of the Mo loading (235–264 μmol NH_3/g). However, the amount of strong acid sites (Table 3) increases with the Mo loading.

HAADF-STEM was carried out to investigate the morphologies of Mo species on TiO_2, and the resulting images of TiO_2, 5% MoO_3/TiO_2, and 20% MoO_3/TiO_2 are shown in Figure 5. Besides, EDS mapping results are given in Figures S6 and S7. The MoO_3 nanoclusters (bright dots) are more uniformly dispersed for 5% MoO_3/TiO_2 than for 20% MoO_3/TiO_2. The nanocluster size distributions of 5% MoO_3/TiO_2 and 20% MoO_3/TiO_2 are
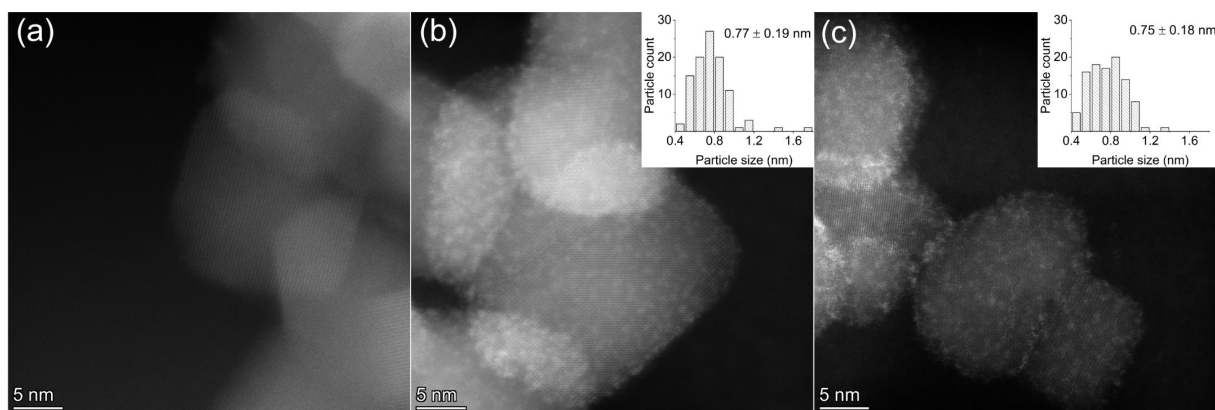
ChemCatChem

Research Article
doi.org/10.1002/cctc.202200297

Chemistry Europe
European Chemical
Societies Publishing

Figure 5. HAADF-STEM images of (a) TiO_2, (b) 5% MoO_3/TiO_2, and (c) 20% MoO_3/TiO_2

provided in Figure 5 and reveal that the average MoO_3 nanocluster sizes are about 0.76 nm and similar for both catalysts. XRD measurements also indicate the presence of larger MoO_3 crystallites (> 30 nm) at higher Mo loadings. Surprisingly, these crystallites are not visible in the HAADF-STEM images. A possible reason is the presence of the TiO_2 support nanoparticles, which have similar particle sizes, which hampers detection. Similar observations (XRD versus HADDF-STEM) were made by Toyao et al.[51] for 30% MoO_3 on a TiO_2 (P25).

2.2.2. Catalytic experiments using guaiacol

The catalytic demethoxylation experiments using TiO_2 (P25) supported MoO_3 catalysts with different MoO_3-loadings were conducted in the same fixed-bed reactor used for the support screening experiments (380°C, 20 bar, WHSV = 0.5 h^{-1}, 5 wt% guaiacol in toluene). The conversion and selectivity data after a TOS of 4 h are given in Figure 6. For comparison, the results for 1% Au/TiO_2, a well-known catalyst for demethoxylation of guaiacol and 4-n-propylguaiacol, have been added as well.[18,20]

Guaiacol conversion for all Mo-supported catalysts is high and above 95%. Unconverted guaiacol was still detected in the outlet, indicating that the experiments were not performed at quantitative conversion. Bulk TiO_2 is also active, but the conversion of guaiacol is much lower (57%) than found for the MoO_3 based catalysts. Unsupported MoO_3 is also very active, and the conversion is similar to the supported ones, though the selectivity to demethoxylated products is low (*vide infra*). Of interest is the observation that the Mo catalysts at the prevailing conditions are as active when considering conversion as a well-known precious metal catalyst (Au/TiO_2).
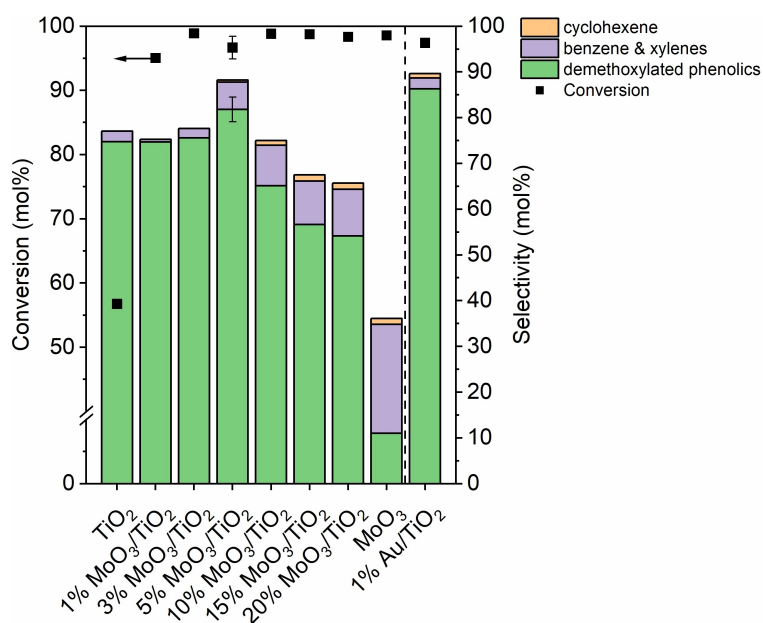
Figure 6. Conversion and selectivity values for the demethoxylation of guaiacol using TiO_2, 1 – 20% MoO_3/TiO_2, MoO_3, and 1% Au/TiO_2 catalysts. Reaction conditions: T = 380°C, P = 20 bar, WHSV = 0.5 h^{-1}, 5 wt% guaiacol in toluene, and TOS = 4 h. The detailed product distributions are shown in Figure S8.

ChemCatChem

Research Article
doi.org/10.1002/cctc.202200297

Chemistry
Europe
European Chemical
Societies Publishing

Demethoxylated phenols like the parent phenol, cresols and xylenols, as well as aromatics (benzene, and xylenes) are the major component groups formed when using the supported Mo catalysts. A detailed overview including minor components is given in Figure S8. The balance closure on molar basis is not quantitative, and this is likely due to the formation of gas-phase components, some coke on the catalyst (*vide infra*), some minor products in the GC that could not be quantified accurately, and the formation of some soluble oligomeric products, as confirmed by GPC (Figure S9).

Product selectivity is highly dependent on the Mo loading. The highest amounts of low molecular weight demethoxylated products, the desired products in this study, are obtained when using low Mo loadings, with 5% Mo being the most favorable one. The use of 5% MoO_3/TiO_2 resulted in 97% conversion of guaiacol and 82% selectivity to demethoxylated phenolics (including phenol and methyl-, dimethyl-, trimethylphenol). As such, the yield of demethoxylated phenolics is as high as 79%, which is in the range for precious metal catalysts (Pt–Sn/CNF/Inconel, Pd/C, and Au/TiO_2 with 92–99% conversion and 79–84% selectivity)[16,17,19] and some best of non-precious metal catalysts reported so far (FeO_x/CeO_2, MoO_3, and MoO_2/AC with 96–100% conversion and 84–97% selectivity)[23,27,28] for guaiacol demethoxylation. The use of the 5% MoO_3/TiO_2 also resulted in the highest phenol yield (38%) within the catalyst series investigated, including the benchmark Au/TiO_2 (36%).

At low MoO_3 loading (1–5%), the major products are demethoxylated phenolics, and their selectivity increases with the Mo loading. At higher Mo loadings (10-20% MoO_3 loading), the amounts of fully deoxygenated products (benzene, xylene, and cyclohexene) increase significantly. In addition, molar balance closure becomes much worse, and more unidentified products, most likely soluble oligomers (shown in Figure S9) and coke are formed. The amounts of these non-GC detectable byproducts appear to be related to the strong acidity of the catalyst, see Figure 7 for details. Thus, the observed reduction in the selectivity at high loadings is most likely due to the oligomerization of reactive intermediates on the surface catalyzed by strong acid sites.

2.2.3. Catalyst structure-performance relations

With the catalyst characterization data and catalytic performance data available, we have attempted to identify correlations between structure and performance. A clear trend was found between the surface area according to BET and the selectivity to demethoxylated phenolics, see Figure 8 for details. It is evident that a higher surface area leads to improved performance. It is well possible that a high surface area is beneficial for the creation of Ov–I sites on the support, which are known to be important species in the catalytic cycle (*vide infra*).

The selectivity to demethoxylated phenols also correlates with the relative amounts of weak and medium acid sites, see Figure 9. it appears that these acidic sites have a very positive effect on the selectivity to the desired compounds. Apparently, these play an important role in the catalytic cycle and may be
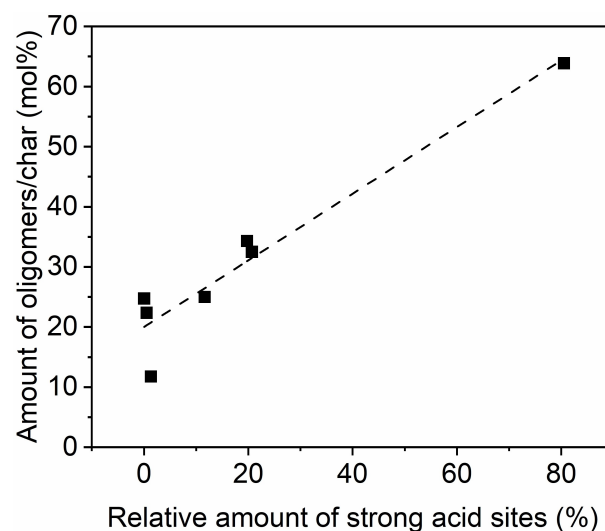
Figure 7. Correlation between the amounts of oligomers/char and relative amount of strong acid sites in the acid site distribution for the MoO_3 catalysts.
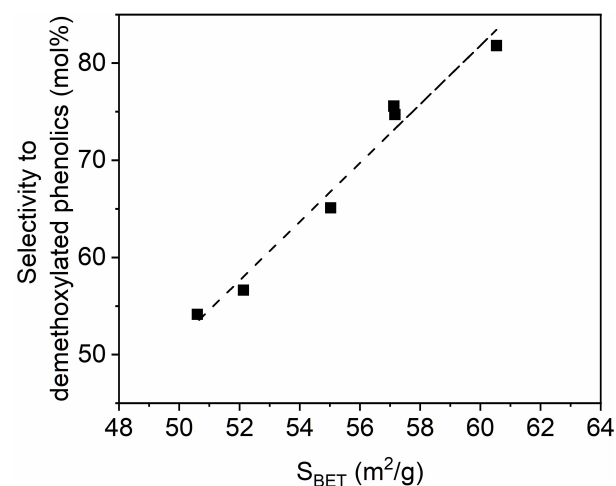
Figure 8. Selectivity to demethoxylated phenolics versus surface area for the MoO_3 catalysts.

involved in activation of guaiacol on the active species of the catalysts (*vide infra*).

In addition, a good correlation was found between the amount of Ov per Mo atom and the selectivity of demethoxylated phenolics (Figure 10). The best selectivity is obtained at the highest concentration of Ov per Mo. However, as stated above, two different types of Ov are expected to be involved in the catalytic cycle (Ov I and Ov II), and these may also affect selectivity. For instance, based on the observed selectivity patterns versus the Mo loading (more aromatics like benzene and xylenes at higher Mo-loadings), particularly the Ov II sites may be involved in deep hydrodeoxygenation by Ph-OH cleavage (*vide infra*).

ChemCatChem

Research Article
doi.org/10.1002/cctc.202200297

**Chemistry
Europe**
European Chemical
Societies Publishing
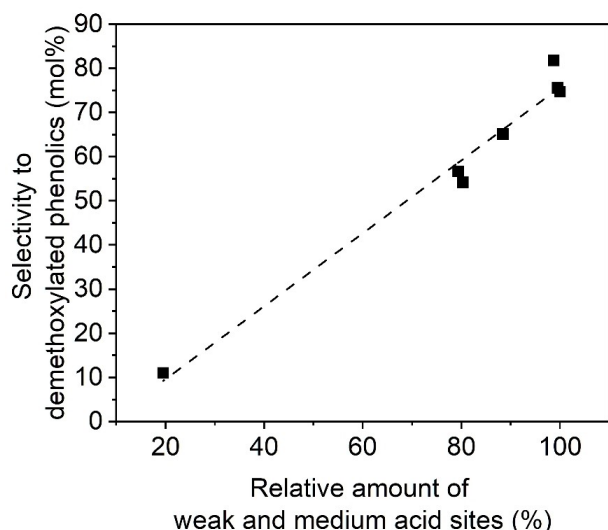
Figure 9. Selectivity to demethoxylated phenolics versus relative amounts of weak and medium active sites for the MoO$_3$ catalysts.

2.2.4. Mechanistic implications

Based on the catalyst characterization studies in combination with the selectivity patterns for the catalysts with different Mo loadings and literature precedents, a mechanism is proposed for guaiacol demethoxylation on MoO$_3$/TiO$_2$ catalysts (Figure 11). It assumes that H$_2$ is adsorbed on particularly reduced MoO$_x$ species and dissociates to provide chemisorbed hydrogen.[48,49] Subsequent reaction of the latter with surface TiO$_2$ creates Ov I sites on the TiO$_2$ support Guaiacol is activated at these sites and demethoxylated to form phenol. It was found

that particularly weak and medium acidic sites play a role and have a positive effect on the selectivity. It is well possible that both the mode of coordination of guaiacol to the support as well as the subsequent activation of guaiacol may be positively affected by nearby acidic sites and that particularly the weak and medium acid sites are important in this respect to form (alkylated) phenols.

The exact formation mechanism for alkylated phenol formation, which are detected experimentally in substantial amounts, is still under debate. It has been proposed that the initially formed phenol may react with guaiacol to form methylated phenols and catechol.[18,21] However, catechol is not detected throughout the reaction, meaning that either this pathway is not taking place to a considerable extent or that the catechol is a very reactive intermediate that is rapidly converted to other products. An alternative mechanism involves Friedel-Crafts-type reaction where CH$_3^+$ species are involved and which are active in intra- or inter-molecular methylation reactions.[23,52]

At higher Mo loadings the selectivity to alkylphenols drops and more aromatics like benzene and xylenes are formed, as well as oligomers and char. It is well possible that particularly reduced MoO$_x$ sites (Ov II) are active for the hydrodeoxygenation of intermediate alkylated phenolics and the parent phenol to aromatics. An alternative explanation is related to the size of the MoO$_x$ nanocrystallites on the TiO$_2$ support. At lower Mo loadings, small isolated MoO$_3$ or slightly agglomerated MoO$_3$ clusters are present (XRD, TEM), while the larger ones are more dominant at higher loadings and these may be involved in deep hydrodeoxygenation to aromatic products like benzene and xylenes. However, we do not yet have hard evidence for any of these hypotheses.

Several studies have also proposed that oxycarbohydride (MoO$_x$C$_y$H$_z$) or oxycarbide (MoO$_x$C$_y$) phases of Mo are active for
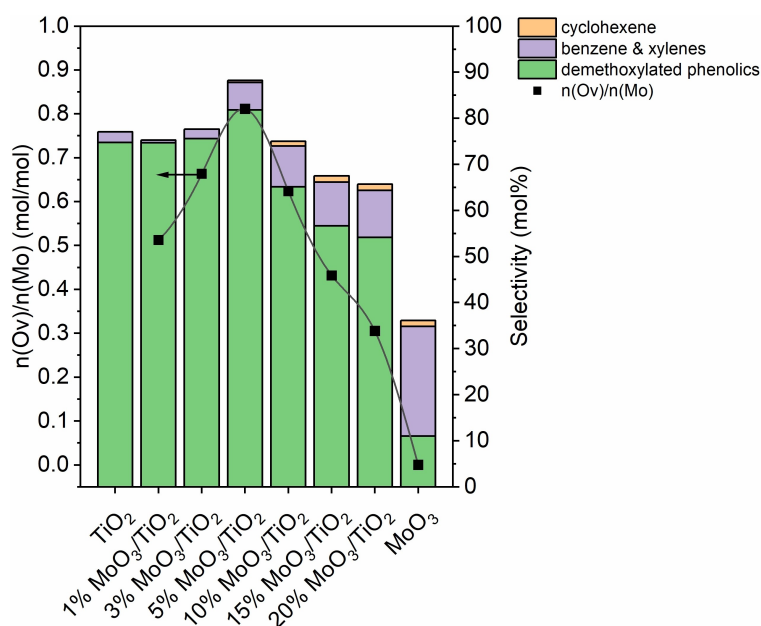
Figure 10. Correlation between the selectivity of demethoxylated phenols and the n(Ov)/n(Mo). n(Ov)/n(Mo) stands for the ratio between the concentration of Ov (n(Ov), μmol/g) and the Mo content in the catalyst (n(Mo), μmol/g).

ChemCatChem

Research Article
doi.org/10.1002/cctc.202200297
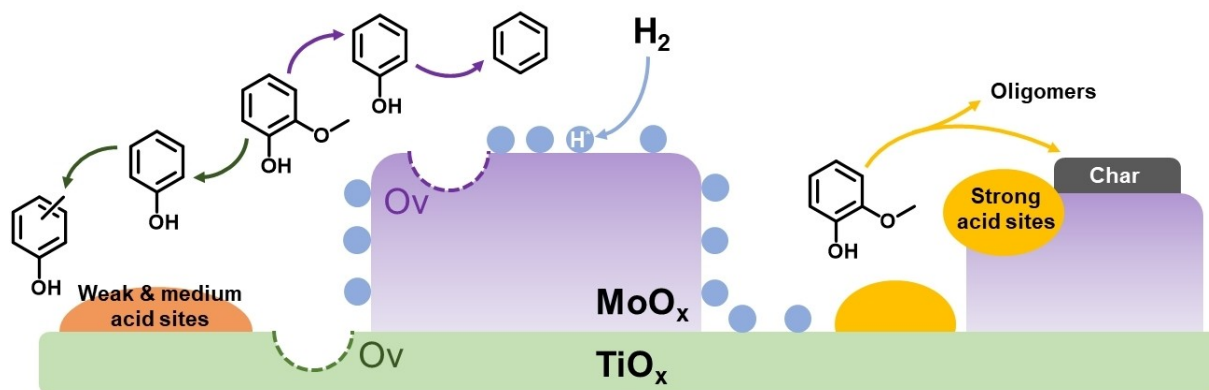
Chemistry
Europe
European Chemical
Societies Publishing

Figure 11. Proposed mechanism of guaiacol hydrodeoxygenation over MoO_3/TiO_2 catalysts.

hydrodeoxygenation,[14,53,54] but these phase were not observed on spent catalysts in this study (*vide infra*). However, the presence of such $MoO_xC_yH_z$ or MoO_xC_y phases cannot be ruled out either because these phases could be amorphous in nature or the average size is below the detection limit of XRD.[54,55] The strong acid sites on the catalysts are assumed to be responsible for the formation of oligomers and ultimately to char. As a result, the highest selectivity to demethoxylated phenolics as found for the 5% MoO_3/TiO_2 catalyst is ascribed to a proper balance between Ov I and type of acid sites, leading to mainly demethoxylated products like phenol and alkylated phenols while subsequent hydrodeoxygenation to aromatics and oligomerization/condensation are retarded.

2.2.5. Effect of process conditions on catalyst performance

The effect of process conditions like temperature (300–380 °C) and WHSV (0.5–2 h^{-1}) was investigated for the best catalysts in the series (5% MoO_3/TiO_2), and the results are given in (Figure 12). As expected, the conversion increases from about 20% to 95+% when increasing the temperature from 300 to 380 °C (WHSV of 0.5 h^{-1}). The selectivity to monomeric, GC detectables increases with temperature, though slightly higher amounts of deoxygenated aromatics like benzene and xylenes are detected at higher temperatures. The conversion depends on the WHSV (temperature set at 380 °C) with, as expected, higher conversions at lower WHSV's (Figure 12). Thus, it can be concluded that the highest yields of the desired demethoxylated phenols like phenol and alkylphenols are attainable at the highest temperature and lowest WHSV in the range.
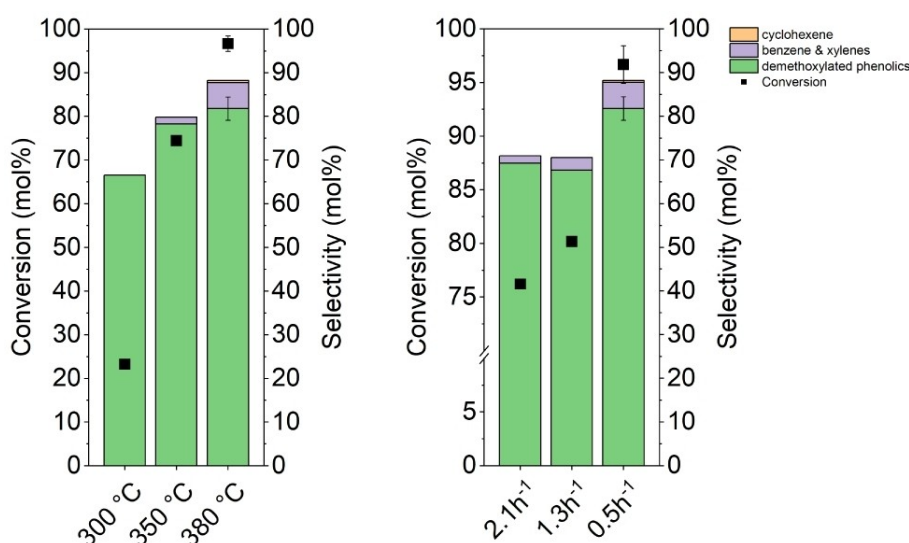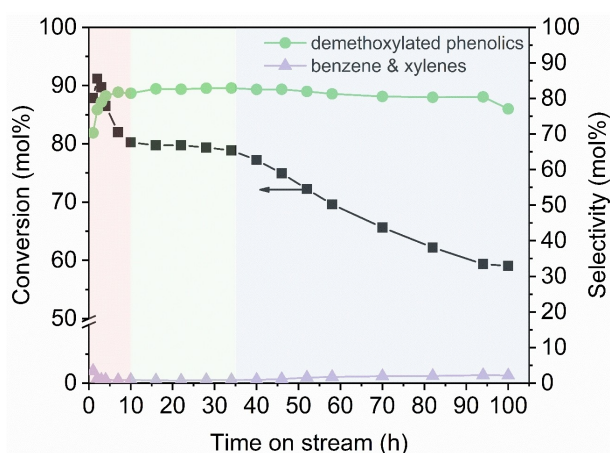

Figure 12. Guaiacol conversion and selectivity for the 5% MoO_3/TiO_2 catalyst as a function of temperature (left, 20 bar, WHSV = 0.5 h^{-1}, 5 wt% guaiacol in toluene, and TOS = 4 h) and WHSV (right, 380 °C, 20 bar, 5 wt% guaiacol in toluene, and TOS = 4 h). Detailed product distributions are shown in Figure S10.

ChemCatChem

Research Article
doi.org/10.1002/cctc.202200297

**Chemistry
Europe**

European Chemical
Societies Publishing

2.2.6. Catalyst stability for the 5% MoO₃ on TiO₂ catalyst

The stability of the 5% MoO₃ on TiO₂ catalyst was tested in the continuous set-up for a TOS of 100 h at 350 °C, 20 bar and a WHSV of 1 h⁻¹ using guaiacol dissolved in toluene (5 wt%) as the feed and the results are given in Figure 13. The conversion is a function of the TOS and drops from about 90% to 60% after 100 h, indicative of some catalyst deactivation. A better inspection of Figure 13 shows three distinct stages *viz.* a relatively large drop within 10 h TOS, followed by a stable stage at about 80% conversion between 10 and 35 h, and finally a gradual drop in conversion to a final value of 30%. Remarkably, the selectivity to demethoxylated phenols is high and up to 80% throughout the experiment. To gain some insights into the origin of catalyst deactivation, the spent catalyst was analyzed using TGA and ICP-OES. TGA analyses show a weight

loss of around 27 wt% between 300 and 550 °C when the spent catalyst is oxidized in air (Figure S11), and this weight loss is most likely associated with the presence of coke on the catalyst. As such, at least part of the deactivation phenomena may be explained by coke formation on the catalyst. In addition, the amount of MoO₃ in the catalyst formulation is significantly reduced (from 4.5 to 3.9 wt%) after the reaction, indicative of some Mo leaching. Speculatively, the drop in activity in the first stage may be by leaching of loosely bound Mo species on the catalyst surface, while the rather small and slow decrease in activity at extended TOS is due to coke formation on the catalyst surface.

To assess the possibility of carburation of the Mo-surface and the formation of oxycarbide and oxycarbohydride containing phases during the reaction, the spent catalyst with the highest Mo amount was analyzed by XRD. The results are given in Figure S12 and show that clear peaks from such phases are absent.[14] However, on the basis of the findings, the involvement of carburized Mo species cannot be excluded as these could be either amorphous in nature or the average size is below the detection limit of XRD.

Figure 13. Catalyst performance versus TOS for the 5% MoO₃/TiO₂ catalyst (350 °C, 20 bar, WHSV of 1 h⁻¹, 5 wt% guaiacol in toluene as a reactant).

2.2.7. Catalytic experiments using 4-n–propylguaiacol

The solvent-free demethoxylation of 4-n-propylguaiaocol, a major product in the bioliquids obtained from the reductive catalytic fractionation of lignin, was conducted in the continuous set-up using the 5% MoO₃/TiO₂ catalyst at 350 °C, 20 bar, and WHSV values between 0.78 and 6.22 h⁻¹. The results are given in Figure 14 and show that the highest conversion (90%) was obtained at a WHSV of 0.78 h⁻¹. The main products are demethoxylated phenolics (72%) like 2-n-propylphenol, 4-n-propylphenol, and methylated propylphenol (2-sec-butylphenol and 4-sec-butylphenol). A minor GC detectable product is
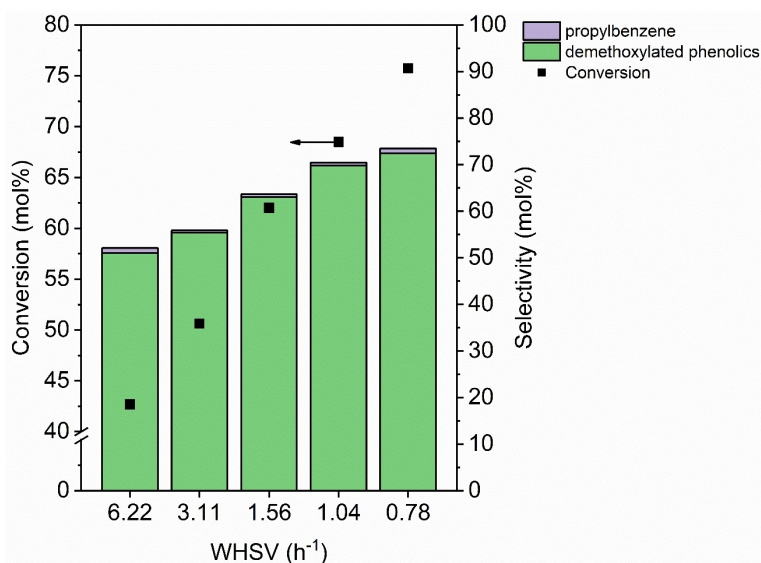
Figure 14. 4-n-propylguaiacol conversion and selectivity versus WHSV over 5% MoO₃/TiO₂. Reaction conditions: T = 350 °C, P = 20 bar, 4-n-propylguaicol as a reactant, and TOS = 4 h. The detailed product distributions are shown in Figure S13.

propylbenzene (about 1%), and detailed product selectivities are provided in Figure S13. As for experiments with guaiacol, the mole balance is not quantitative due to oligomerization reactions and char formation, which was also supported by GPC (Figure S14) and TGA measurements on spent catalysts (Figure S15).

2.2.8. Catalytic experiments using a crude feed (Pyoil) containing methoxylated phenols

Performance of the 5% MoO_3/TiO_2 catalyst for a bioliquid enriched in methoxylated phenols (Pyoil), produced in a pilot plant for pyrolysis oil fractionation, was tested in the continuous set-up at 350 °C, 20 bar, a WHSV of 1 h^{-1}, with the Pyoil dissolved in toluene (5 wt%). Before use, the feed was analyzed using GC and GCxGC chromatography (Figure S16) to gain insight into the molecular composition. The amounts of phenolics in Pyoil are shown in Table 4 and reveal that guaiacol (15.8 wt%), 4-methyguaiacol (32.1 wt%), and 4-ethylguaiacol (8.9 wt%) are the major components.

The experiments in the continuous set-up were carried out without major operational issues for a TOS of 4 h and 8.2 g of the product was obtained. The latter was analyzed using GC, GC x GC, and ^{13}C-NMR to obtain insights into the molecular composition. The GCxGC chromatogram of the product (Figure S16) differs considerably from that of the feed and shows the presence of significant amounts of demethoxylated products like phenol, 2-methylphenol, 4-methylphenol, and 2,4-dimethylphenol. A ^{13}C-NMR spectrum (Figure S17) confirms that near-complete demethoxylation was achieved. The GC data were further quantified using GC-FID, and relevant data (conversions of individual components and product selectivities) are reported in Table 5. It shows that most of the methoxy groups in the real feed are removed and that the main products are phenol and alkylated phenols. Thus, it can be concluded that demethoxylation of a real feed is well possible using the MoO_3/TiO_2 catalysts.

3. Conclusions

In this study, a series of supported MoO_3 catalysts were investigated in a continuous fixed-bed reactor for the selective demethoxylation of guaiacols by an HDO approach to preferably phenol and alkylated phenols. The Mo catalyst with the TiO_2 (P25) support shows the best performance with 82% selectivity to demethoxylated phenolics (including phenol and methyl-, dimethyl-, trimethylphenol) at 97% guaiacol conversion. As such, cheap non-precious metals such as MoO_3 on an appropriate support, and preferably TiO_2 (P25), also have the potential to be used for catalytic demethoxylation purposes. Catalyst stability was shown to be reasonable, with a drop in conversion from 90 + % to 60% for a TOS of 100 h.

The best catalyst was also successfully applied for the demethoxylation of 4-n-propylguaiacol and even a phenolic enriched fraction of pyrolysis oil, showing its high feedstock flexibility. The catalysts were characterized in detail and a reaction network and mechanistic proposal at a catalyst level are provided to explain the experimental results. It was shown that higher surface areas, higher amounts of weak and medium acid sites, and intermediate Ov concentrations are preferred when considering selectivity to the desired demethoxylated products. It is speculated that the size of the MoO_x nanocrystallites on the TiO_2 support also influences the selectivity of the reaction, with small isolated MoO_3 or slightly agglomerated MoO_3 clusters favoring demethoxylation, while the larger ones are involved in deep hydrodeoxygenation to aromatic products like benzene and xylenes. Future research is in progress to increase the parent phenol yield by combining demethoxylation and dealkylation strategies, and these will be reported in due course.

Experimental section

Materials

TiO_2 (P25, $\geq$ 99.5% trace metals basis, 21 nm primary particle size), TiO_2 ($\geq$ 99%, average diameter of 156 nm), ZrO_2 (99% trace metals basis, 5 μm), Nb_2O_5 (99.99% trace metals basis), CeO_2 ($<$ 25 nm particle size), SiO_2 (99.5% trace metals basis, 10–20 nm particle size), ammonium molybdate tetrahydrate (99.98% trace metals basis), guaiacol ($\geq$ 99%), 4-n-propylguaiacol ($\geq$ 99%), 4-n-propyl-

Table 4. Chemical composition of the Pyoil (GC-FID).

Compounds	[wt%]
Phenol	0.7
2-Methylphenol	1.7
4-Methylphenol	3.0
Guaiacol	15.8
Dimethylphenol	2.8
3-Methylguaiacol	1.8
4-Methylguaiacol	32.1
Dimethoxytoluene	1.5
4-Ethylguaiacol	8.9
Eugenol	3.5
4-Propylguaiacol	1.5
Others[a]	26.7

[a] mainly GC undetectable compounds and oligomers.

Table 5. Conversion and selectivity for the hydrotreatment of Pyoil over 5% MoO_3/TiO_2. Reaction conditions: T = 350 °C, P = 20 bar, WHSV = 1 h^{-1}, 5 wt% real feed in toluene as a reactant, and TOS = 4 h.

Compounds	Conversion [mol%]	Selectivity [mol%]
Guaiacol	92	–
3-Methylguaiacol	100	–
4-Methylguaiacol	94	–
Dimethoxytoluene	100	–
4-Ethylguaiacol	93	–
Eugenol	78	–
4-Propylguaiacol	100	–
Phenol	–	12.7
Methylphenols	–	32.3
Dimethylphenols	–	24.9
Higher methylated phenols	–	16.1
Benzene and Ethylbenzene	–	1.51

phenol (99%), 2-*sec*-butylphenol (98%), 4-*n*-propyl anisole ($\geq$ 99%), benzene ($\geq$ 99.7%), cyclohexene (99%) were supplied by Sigma-Aldrich. γ-Al$_2$O$_3$ (99.97% metal basis) purchased from Alfa Aesar. Toluene ($\geq$ 99%) and tetrahydrofuran (THF) stabilized with BHT (for analysis) were obtained from Avantor and Boom B.V., respectively. Phenol ($>$99.5%), 4-methylphenol ($>$99.0%), 2,3-dimethylphenol ($>$98.0%), 2,3,6-trimethylphenol ($>$98.0%), 1,2-dimethoxybenzene ($>$99.0%), 4-methylguaiacol ($>$98.0%), catechol ($>$99.0%), *n*-propylbenzene ($>$99.0%), decane ($>$99.0%), and dodecane ($>$99.0%) were purchased from TCI. p-Xylene (99%) and, o-xylene (99%) were obtained from abcr GmbH.

A bioliquid enriched in guaiacols, abbreviated as Pyoil, was provided from the Biomass Technology Group B.V. and was isolated from pyrolysis oil by fractionation on pilot plant scale (3 t/d of pyrolysis oil input).

Catalyst synthesis

Supported MoO$_3$ catalysts were prepared using the incipient wetness impregnation method. Typically for the synthesis of a batch of catalyst with a loading of 5 wt% MoO$_3$, ammonium molybdate tetrahydrate (0.1291 g) was dissolved in an appropriate amount of Milli-Q water (corresponding to the measured water volume for quantitative wetting of the support). This solution was added dropwise to the support (2.000 g) and mixed vigorously. The mixture was dried at 100 °C for 12 h, followed by calcination at 550 °C (2 °C min^{-1}) for 4 h in static air. The catalysts were pelletized, crushed, and sieved to a 100–200 μm fraction before testing. 1 wt% Au/TiO$_2$ was prepared by a deposition-precipitation method using urea[36]. The sample was calcined at 350 °C (2 °C min^{-1}) for 2 h, pelletized, crushed, and sieved to a 100–200 μm fraction before use. The catalysts were characterized by XRD, ICP-OES, N$_2$ physisorption, H$_2$-TPR, NH$_3$-TPD, oxygen storage capacity (OSC) measurements, HAADF-STEM, and TGA. The details are provided in the supporting information.

Catalytic experiments

The catalytic hydrodeoxygenation of guaiacol, 4-*n*-propylguaiacol, and Pyoil was carried out in a continuous down-flow fixed-bed reactor (stainless steel) with an outer diameter of 6.35 mm and an inner diameter of 4.55 mm. Typically, the supported MoO$_3$ catalyst (100 mg) was diluted with the corresponding support particles (200 mg, 100–200 μm) and then loaded into the reactor. An experiment was started by increasing the reactor pressure to 20 bar using H$_2$ (10 mL/min), followed by heating the reactor to the desired temperature. After that, the reactant, either dissolved in toluene (5 wt%, when using guaiacol or the Pyoil) or neat (4-*n*-propylguaiacol) was introduced to the reactor by an HPLC pump at the desired Weighted Hourly Space Velocity (WHSV, h^{-1}). The WHSV was calculated based on the reactant flow rate (F_g, in g/h) and the catalyst weight (*w*, in g, fixed at 0.1 g) as shown in Equation (1).

$$WHSV = F_g/w \qquad (1)$$

The reaction products were separated in a gas-liquid separator, and condensable products were collected at 1 h intervals. The product composition was determined at a Time on Stream (TOS) of 4 h using off-line GC-MS and GC-FID. Product characterization and quantification details involving GC and GPC analyses are provided in the supporting information.

The conversion of a feed component *g* and selectivity for a product *i* were calculated on a molar basis [Eqs. (2) and (3)].

$$X_g \ (\%) = (C_{g,0} - C_g)/C_{g,0} \times 100 \qquad (2)$$

$$S_i \ (\%) = C_i/(C_{g,0} - C_g) \times 100 \qquad (3)$$

Here, $C_{g,0}$ is the concentrations (mol/L) of guaiacol or 4-*n*-propylguaiacol in the feed and C_g is the concentration (mol/L) in the outlet of the reactor, and C_i is the concentration (mol/L) of a product *i* in the outlet of the reactor. The presence of demethoxylated phenols in the Pyoil were considered when calculating the product selectivity for Pyoil (see supporting information).

Conflict of Interest

The authors declare no conflict of interest.

Data Availability Statement

The data that support the findings of this study are available in the supplementary material of this article.

Keywords: demethoxylation · guaiacol · MoO$_3$ catalysts · titania · pyrolysis oil

[1] C. Zhengwen, E. Jan, D. Michael, C. M. T. W. Guang-Hui, H. Eleni, L. Angelos, R. Roberto, S. Ferdi, *Angew. Chem. Int. Ed.* **2017**, *56*, 2334–2339; *Angew. Chem.* **2017**, *129*, 2374–2379.
[2] N. Ji, X. Diao, X. Li, Z. Jia, Y. Zhao, X. Lu, C. Song, Q. Liu, C. Li, *Ind. Eng. Chem. Res.* **2020**, *59*, 17287–17299.
[3] E. Furimsky, *Appl. Catal. A* **2000**, *199*, 147–190.
[4] J.-S. Kim, *Bioresour. Technol.* **2015**, *178*, 90–98.
[5] A. S. Pollard, M. R. Rover, R. C. Brown, *J. Anal. Appl. Pyrolysis* **2012**, *93*, 129–138.
[6] T. Schulzke, S. Conrad, J. Westermeyer, *Biomass Bioenergy* **2016**, *95*, 287–295.
[7] S. Papari, K. Hawboldt, *Fuel Process. Technol.* **2018**, *180*, 1–13.
[8] H. Heeres, E. J. Leijenhorst, R. Ongena, L. Van de Beld, in *Eur. Biomass Conf. Exhib. Proc.*, ETA-Florence Renewable Energies, **2019**, pp. 1894–1898.
[9] A.-C. Johansson, K. Iisa, L. Sandström, H. Ben, H. Pilath, S. Deutch, H. Wiinikka, O. G. W. Öhrman, *J. Anal. Appl. Pyrolysis* **2017**, *123*, 244–254.
[10] R. Rinaldi, R. Jastrzebski, M. T. Clough, J. Ralph, M. Kennema, P. C. A. Bruijnincx, B. M. Weckhuysen, *Angew. Chem. Int. Ed.* **2016**, *55*, 8164–8215; *Angew. Chem.* **2016**, *128*, 8296–8354.
[11] Y. Jing, Y. Wang, *Front. Chem. Eng.* **2020**, *2*, 1–7.
[12] D. C. Elliott, T. R. Hart, *Energy Fuels* **2009**, *23*, 631–637.
[13] M. Saidi, F. Samimi, D. Karimipourfard, T. Nimmanwudipong, B. C. Gates, M. R. Rahimpour, *Energy Environ. Sci.* **2014**, *7*, 103–129.
[14] T. Prasomsri, M. Shetty, K. Murugappan, Y. Román-Leshkov, *Energy Environ. Sci.* **2014**, *7*, 2660–2669.

[15] Z. Luo, Z. Zheng, Y. Wang, G. Sun, H. Jiang, C. Zhao, *Green Chem.* **2016**, *18*, 5845–5858.

[16] M. Á. González-Borja, D. E. Resasco, *Energy Fuels* **2011**, *25*, 4155–4162.

[17] J. Sun, A. M. Karim, H. Zhang, L. Kovarik, X. S. Li, A. J. Hensley, J.-S. McEwen, Y. Wang, *J. Catal.* **2013**, *306*, 47–57.

[18] J. Mao, J. Zhou, Z. Xia, Z. Wang, Z. Xu, W. Xu, P. Yan, K. Liu, X. Guo, Z. C. Zhang, *ACS Catal.* **2017**, *7*, 695–705.

[19] T.-S. Nguyen, D. Laurenti, P. Afanasiev, Z. Konuspayeva, L. Piccolo, *J. Catal.* **2016**, *344*, 136–140.

[20] X. Huang, J. M. Ludenhoff, M. Dirks, X. Ouyang, M. D. Boot, E. J. M. Hensen, *ACS Catal.* **2018**, *8*, 11184–11190.

[21] K. Liu, P. Yan, H. Jiang, Z. Xia, Z. Xu, S. Bai, Z. C. Zhang, *J. Catal.* **2019**, *369*, 396–404.

[22] X. Wang, P. Wu, Z. Wang, L. Zhou, Y. Liu, H. Cheng, M. Arai, C. Zhang, F. Zhao, *ACS Sustainable Chem. Eng.* **2021**, acssuschemeng.0c07292.

[23] C. Li, Y. Nakagawa, M. Tamura, A. Nakayama, K. Tomishige, *ACS Catal.* **2020**, 14624–14639.

[24] X. Zhang, P. Yan, B. Zhao, Z. C. Zhang, *Catal. Sci. Technol.* **2021**, *11*, 297–311.

[25] M. B. Griffin, F. G. Baddour, S. E. Habas, C. P. Nash, D. A. Ruddy, J. A. Schaidle, *Catal. Sci. Technol.* **2017**, *7*, 2954–2966.

[26] X. Zhang, J. Tang, Q. Zhang, Q. Liu, Y. Li, L. Chen, C. Wang, L. Ma, *Catal. Today* **2019**, *319*, 41–47.

[27] X. Diao, N. Ji, T. Li, Z. Jia, S. Jiang, Z. Wang, C. Song, C. Liu, X. Lu, Q. Liu, *J. Catal.* **2021**, *401*, 234–251.

[28] Z. Cai, F. Wang, X. Zhang, R. Ahishakiye, Y. Xie, Y. Shen, *J. Mol. Catal.* **2017**, *441*, 28–34.

[29] J. Chang, T. Danuthai, S. Dewiyanti, C. Wang, A. Borgna, *ChemCatChem* **2013**, *5*, 3041–3049.

[30] S. Song, J. Zhang, N. Yan, *Fuel Process. Technol.* **2020**, *199*, 106224.

[31] Y. Liao, S. Koelewijn, G. Van den Bossche, J. Van Aelst, S. Van den Bosch, T. Renders, K. Navare, T. Nicolaï, K. Van Aelst, M. Maesen, H. Matsushima, J. M. Thevelein, K. Van Acker, B. Lagrain, D. Verboekend, B. F. Sels, *Science* **2020**, *367*, 1385–1390.

[32] S. M. Schimming, O. D. LaMont, M. König, A. K. Rogers, A. D. D'Amico, M. M. Yung, C. Sievers, *ChemSusChem* **2015**, *8*, 2073–2083.

[33] X. Ouyang, X. Huang, M. D. Boot, E. J. M. Hensen, *ChemSusChem* **2020**, *13*, 1705–1709.

[34] I. T. Ghampson, C. Sepúlveda, R. Garcia, B. G. Frederick, M. C. Wheeler, N. Escalona, W. J. DeSisto, *Appl. Catal. A* **2012**, *413–414*, 78–84.

[35] S. Liu, H. Wang, K. J. Smith, C. S. Kim, *Energy Fuels* **2017**, *31*, 6378–6388.

[36] R. Zanella, S. Giorgio, C. H. Shin, C. R. Henry, C. Louis, *J. Catal.* **2004**, *222*, 357–367.

[37] G. Tsilomelekis, A. Christodoulakis, S. Boghosian, *Catal. Today* **2007**, *127*, 139–147.

[38] K. Liu, X. Huang, E. A. Pidko, E. J. M. Hensen, *Green Chem.* **2017**, *19*, 3014–3022.

[39] C. Ranga, V. I. Alexiadis, J. Lauwaert, R. Lødeng, J. W. Thybaut, *Appl. Catal. A* **2019**, *571*, 61–70.

[40] M. Shetty, K. Murugappan, W. H. Green, Y. Román-Leshkov, *ACS Sustainable Chem. Eng.* **2017**, *5*, 5293–5301.

[41] H. Zhu, M. Shen, Y. Wu, X. Li, J. Hong, B. Liu, X. Wu, L. Dong, Y. Chen, *J. Phys. Chem. B* **2005**, *109*, 11720–11726.

[42] H. Hu, I. E. Wachs, S. R. Bare, *J. Phys. Chem.* **1995**, *99*, 10897–10910.

[43] J. Li, G. Lu, G. Wu, D. Mao, Y. Guo, Y. Wang, Y. Guo, *Catal. Sci. Technol.* **2014**, *4*, 1268–1275.

[44] C. Hernández Mejía, T. W. Van Deelen, K. P. De Jong, *Nat. Commun.* **2018**, *9*, 1–8.

[45] G. C. Bond, S. F. Tahir, *Appl. Catal. A* **1993**, *105*, 281–288.

[46] S. Boullosa-Eiras, R. Lødeng, H. Bergem, M. Stöcker, L. Hannevold, E. A. Blekkan, *Catal. Today* **2014**, *223*, 44–53.

[47] T. Prasomsri, T. Nimmanwudipong, Y. Román-Leshkov, *Energy Environ. Sci.* **2013**, *6*, 1732.

[48] H. Hu, D. Oliveira de Souza, E. Berrier, J.-F. Paul, C. La Fontaine, V. Briois, S. Cristol, A. Tougerti, *J. Phys. Chem. C* **2019**, *123*, 18325–18335.

[49] T. Len, M. Bahri, O. Ersen, Y. Lefkir, L. Cardenas, I. J. Villar-Garcia, V. Pérez Dieste, J. Llorca, N. Perret, R. Checa, E. Puzenat, P. Afanasiev, F. Morfin, L. Piccolo, *Green Chem.* **2021**, *23*, 7259–7268.

[50] M. S. Zanuttini, B. O. Dalla Costa, C. A. Querini, M. A. Peralta, *Appl. Catal. A* **2014**, *482*, 352–361.

[51] T. Toyao, S. Kayamori, Z. Maeno, S. M. A. H. Siddiki, K.-I. Shimizu, *ACS Catal.* **2019**, *9*, 8187–8196.

[52] C. Li, Y. Nakagawa, M. Yabushita, A. Nakayama, K. Tomishige, *ACS Catal.* **2021**, 12794–12814.

[53] K. Murugappan, E. M. Anderson, D. Teschner, T. E. Jones, K. Skorupska, Y. Román-Leshkov, *Nat. Catal.* **2018**, *1*, 960–967.

[54] J. Zhu, E. A. Uslamin, N. Kosinov, E. J. M. Hensen, *Catal. Sci. Technol.* **2020**, *10*, 3635–3645.

[55] M. Shetty, K. Murugappan, T. Prasomsri, W. H. Green, Y. Román-Leshkov, *J. Catal.* **2015**, *331*, 86–97.